Nitric Acid Uptake and Decomposition on Black Carbon (Soot) Surfaces: Its Implications for the Upper Troposphere and Lower Stratosphere

Wonyong Choi[†] and Ming-Taun Leu*

Earth and Space Sciences Division, Jet Propulsion Laboratory, California Institute of Technology, Pasadena, California 91109

Received: March 26, 1998; In Final Form: June 23, 1998

The uptake and decomposition of HNO_3 on black carbon (soot) surfaces were investigated in order to evaluate the proposal that HNO_3 decomposition on aircraft-generated soot aerosols may alter the NO_x/NO_y partitioning in the upper troposphere and lower stratosphere. The experimental measurements were performed by using a fast flow-tube reactor coupled to a quadrupole mass spectrometer. Black carbon samples used as surrogate material for aircraft soot in this study included Degussa FW2 (an amorphous carbon black comprising medium oxides), graphite, hexane soot, and kerosene soot. The measurements of uptake were performed by varying $P(HNO_3)$ in the range of 5×10^{-7} to 5×10^{-4} Torr at 220 and 295 K. The results are summarized as follows. Significant HNO_3 decomposition was observed on FW2 at 295 K with $P(HNO_3) \geq 1 \times 10^{-4}$ Torr, while it did not occur at 220 K. Similar HNO_3 decomposition behavior on graphite was also observed under the condition of $P(HNO_3) \geq 10^{-4}$ Torr and $T = 295$ K, although the extent of the decomposition was much smaller than that on FW2. The decomposition of HNO_3 on soot produced NO, NO_2, H_2O, oxidized soot surface, and some unidentified volatile products. To explain the observed decomposition behavior at higher partial pressures of HNO_3, a bimolecular HNO_3 decomposition mechanism on soot surfaces was proposed. However, HNO_3 immediately decomposed on an FW2 surface at 503 K even at lower partial pressure ($\sim 10^{-6}$ Torr). On flame-deposited hexane and kerosene soot film, no HNO_3 decomposition was observed up to $P(HNO_3) = 5 \times 10^{-4}$ Torr. Moreover, the uptake and desorption of HNO_3 were reversible at 295 K and irreversible at 220 K. Adsorbed HNO_3 molecules on hexane soot film were saturated to a monolayer coverage at $P(HNO_3) \sim 2 \times 10^{-4}$ Torr according to Langmuir adsorption isotherm; further increase in $P(HNO_3)$ resulted in multilayer adsorption. Under the experimental conditions ($P(HNO_3) = 5 \times 10^{-7}$ Torr and $T = 220$ K), the uptake of HNO_3 was found to involve purely physical adsorption without showing any sign of irreversible decomposition over all black carbon samples. Subsequent heating of the sample following the uptake at 220 K desorbed most of the adsorbed HNO_3 molecules. Physical adsorption of HNO_3 was found to take place on the surface of concentrated H_2SO_4-coated soot at 230 K, but decomposition of HNO_3 took place at 296 K. Finally, the present results suggest that the HNO_3 decomposition on soot aerosols through a direct gas−solid interaction, which was proposed as a possible NO_y-reactivation mechanism in the atmospheric modeling of upper troposphere and lower stratosphere, should be dismissed.

Introduction

Black carbon particles (soot) are formed as a result of incomplete combustion processes and are ubiquitous in the atmosphere.[1,2] The lower troposphere contains plenty of soot particles whose principal sources are fossil fuel and biomass combustion at the ground level.[3,4] In the upper troposphere and lower stratosphere, however, the only significant source of soot is known to be the exhausts of aircraft engines.[5,6] Unlike the other components of atmospheric aerosols, black carbon aerosols have a large optical absorption coefficient and can have a significant impact on radiative balance by direct light absorption.[7] Soot particles are also thought to play an important role as cloud condensation nuclei and may indirectly affect climatic forcing.[8] Furthermore, black carbon aerosols can provide surface sites for heterogeneous atmospheric chemical reactions.

The possibility of heterogeneous atmospheric chemical reactions on black carbon aerosols has been invoked, especially in relation to aircraft-generated soot in the upper troposphere and lower stratosphere. Although the amount of black carbon collected in this altitude (10−11 km) accounts for only a few percent of the total aerosol (soot + sulfate) mass, the black carbon surface area can be up to 50% of the total surface area.[6] The specific heterogeneous reactions on soot that have been most frequently considered as potential perturbations of atmospheric chemical balance are those of SO_2, NO_x, HNO_3, and O_3. It has been reported that SO_2 was oxidized to sulfate on soot particles[9,10] and O_3 reactively decomposed on soot to give O_2, CO, and CO_2 as products.[11,12] Smith and co-workers[13] have investigated NO_2−soot interaction by using a Fourier transform infrared spectrometer to look for the formation of new surface species. It has been also suggested that NO_2 was reduced to NO on black carbon surfaces.[14,15]

Recently, it has been reported that the $[HNO_3]/[NO_x]$ ratios in photochemical models was overestimated by a factor of 5−10 in comparison to tropospheric measurements.[16] To resolve this discrepancy, a heterogeneous reduction of HNO_3 on carbon aerosols forming NO or NO_2

$$HNO_3 + \text{soot surface} \rightarrow NO \text{ or } NO_2 \qquad (1)$$

* Author to whom correspondence should be addressed.
[†] Present address: School of Environmental Engineering, Pohang University of Science and Technology, Pohang, 790-784, Korea.

S1089-5639(98)01647-8 CCC: $15.00
Published on Web 09/09/1998

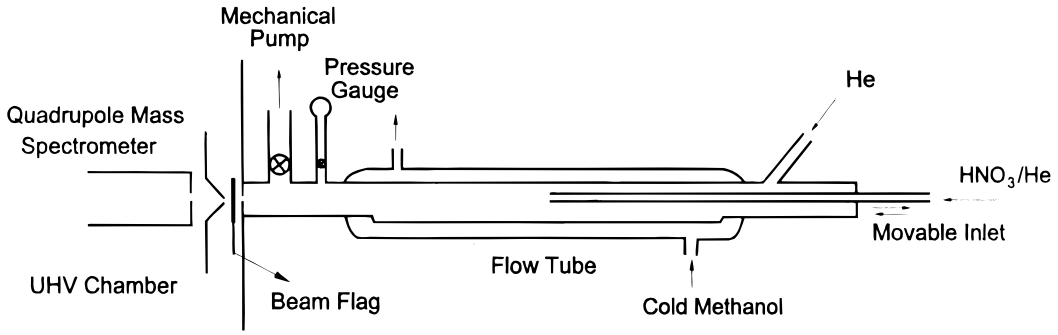

Figure 1. Schematic diagram of the flow reactor coupled to an electron-impact ionization mass spectrometer for the measurements of the HNO_3 uptake on soot surfaces. Both a cylindrical tube reactor and a bottom-flattened tube reactor (shown in the figure) are used in the uptake measurements. Soot samples are either directly flame-deposited on the wall of the cylindrical reactor or laid down on the recessed bottom of the reactor.

has been proposed as a renoxification mechanism on the basis of preliminary laboratory results (see below).[16−18] Since distribution of nitrogen oxides (NO_x) is closely related to photochemical O_3 balance, a possible renoxification of HNO_3 on soot aerosols has direct impact on pathways of ozone production and destruction.

Thlibi and Petit[19] studied HNO_3 reactions on soot in a static reactor at 303 K and reported the decomposition of HNO_3 forming NO and NO_2. Rogaski et al.[20] reported that HNO_3 reacted heterogeneously on amorphous carbon (Degussa FW2) to give NO, NO_2, and H_2O as products with a conversion efficiency of two-thirds. In addition, they obtained a value of $\gamma = 0.038$ at 298 K, which was adopted in atmospheric models.[16−18] However, the experimental conditions of pressures and temperatures employed in the above-mentioned studies were too unrealistic to be extrapolated to the actual atmospheric conditions.

In this article we describe an experimental investigation of physical and chemical interactions of HNO_3 with soot surfaces under widely varying experimental conditions. As surrogate materials for atmospheric carbon aerosols, a commercial carbon black sample (Degussa FW2), graphite, and laboratory-prepared soot samples were used in this study. Decomposition of HNO_3 on soot has been observed under the conditions of its high partial pressure ($\geq 10^{-4}$ Torr) and room temperature, and a relevant mechanism is proposed. The soot reactivity for HNO_3 has been closely investigated under the atmospheric conditions of $P(HNO_3) \sim 10^{-7}$ Torr and $T = 220$ K, and its implications for upper troposphere and lower stratosphere are discussed.

Experimental Section

The uptake measurements were performed by using a fast flow-tube reactor coupled to an electron-impact ionization mass spectrometer (EIMS). The flow reactor/EIMS apparatus has been described in detail earlier,[21] and only a brief summary is presented here. The schematic of the experimental setup is shown in Figure 1. The mass spectrometer housed in an ultrahigh vacuum chamber was operated at a fixed 70 eV electron impact energy and 1−3 mA emission currents. Two flow-tube reactors made of borosilicate were used in this study. A cylindrical tube reactor 21 cm in length and 2.6 cm inside diameter was used for measurements on hexane soot. Another reactor 20 cm long and 2.9 cm^2 in cross-section had a flattened bottom (as shown in Figure 1) in order to hold the samples in place. This reactor was used for measurements on kerosene soot, FW2, and graphite. Helium (Matheson U.H.P.) was used as a main carrier gas in the reactor. The flow rates of He measured by a mass flowmeter (Hastings Instruments) were in the range of 150−450 sccm (standard cubic centimeter per minute). The total pressure in the flow tube, which was monitored by a high-precision capacitance manometer (MKS Instruments, Model 390 HA, 10 Torr full-scale), ranged from 0.3 to 1.0 Torr. The pressure measured at the downstream end of the reactor was corrected (<3%) for the viscous pressure drop between the measuring point and the midpoint of the flow tube.[22] For the low-temperature measurements the flow tube was cooled to ~220 K by circulating chilled methanol through a cooling jacket. The temperature monitored by an iron−constantan thermocouple remained constant within ±1 K during the experiment. A heating tape wrapping around the reactor was used for high-temperature measurements.

Nitric acid was prepared by reacting concentrated H_2SO_4 (96 wt %) with $NaNO_3$ in a vacuum, and the HNO_3 vapor was collected in a Pyrex vessel held at liquid nitrogen temperature. The HNO_3 thus prepared was further purified by vacuum distillation and stored at 76 K. Nitric acid was introduced into the flow reactor by flowing helium through the HNO_3 reservoir vessel in a temperature-controlled bath. The partial pressures of HNO_3 in the flow tube were calculated from the known vapor pressure of HNO_3 at a specific reservoir temperature.[23]

Four different carbon black samples were tested in this study. FW2 (channel type black), which contained about 18% volatiles when heated to 1100 K, was supplied by the Degussa Corp.[24] Graphite powder of 1−2 μm sized particles was purchased from Aldrich. Hexane soot was prepared in the laboratory by burning hexanes (J. T. Baker) which contained mixtures of *n*-hexane, methylpentane, methylcyclopentane, and diethylbutane. Kerosene soot was also prepared in the laboratory by burning kerosene (Aldrich, low-order). The B.E.T. (Brunauer, Emmett, and Teller) surface areas of each sample were measured with powder or substrate-coated forms by using Kr as an adsorptive gas. The measured B.E.T. surface area of each carbon sample, the physical form of sample used in the flow reactor, and the total sample mass in the flow reactor are listed in Table 1.

Various physical forms of carbon black were made out of powder in order to immobilize carbon samples in the flow reactor which was continuously evacuated by a high-capacity mechanical pump. Graphite powder was pressed into disk pellets 1 in. in diameter. If there was a need to increase the surface area in some experiments, the disk pellets were broken into smaller chips. Although the graphite powder was pressed into chips (or pellets) under high pressure (about 10 ton), there was no difference in the measured specific B.E.T. surface area (15 m^2/g) between the powder and chip (or pellet) samples. This implied that each pressed chip (or pellet) was still microporous and that the internal surface of the chips might be available for HNO_3 uptake to a small extent. Since FW2 powder could not be made into disk pellets due to its mechanical brittleness, it

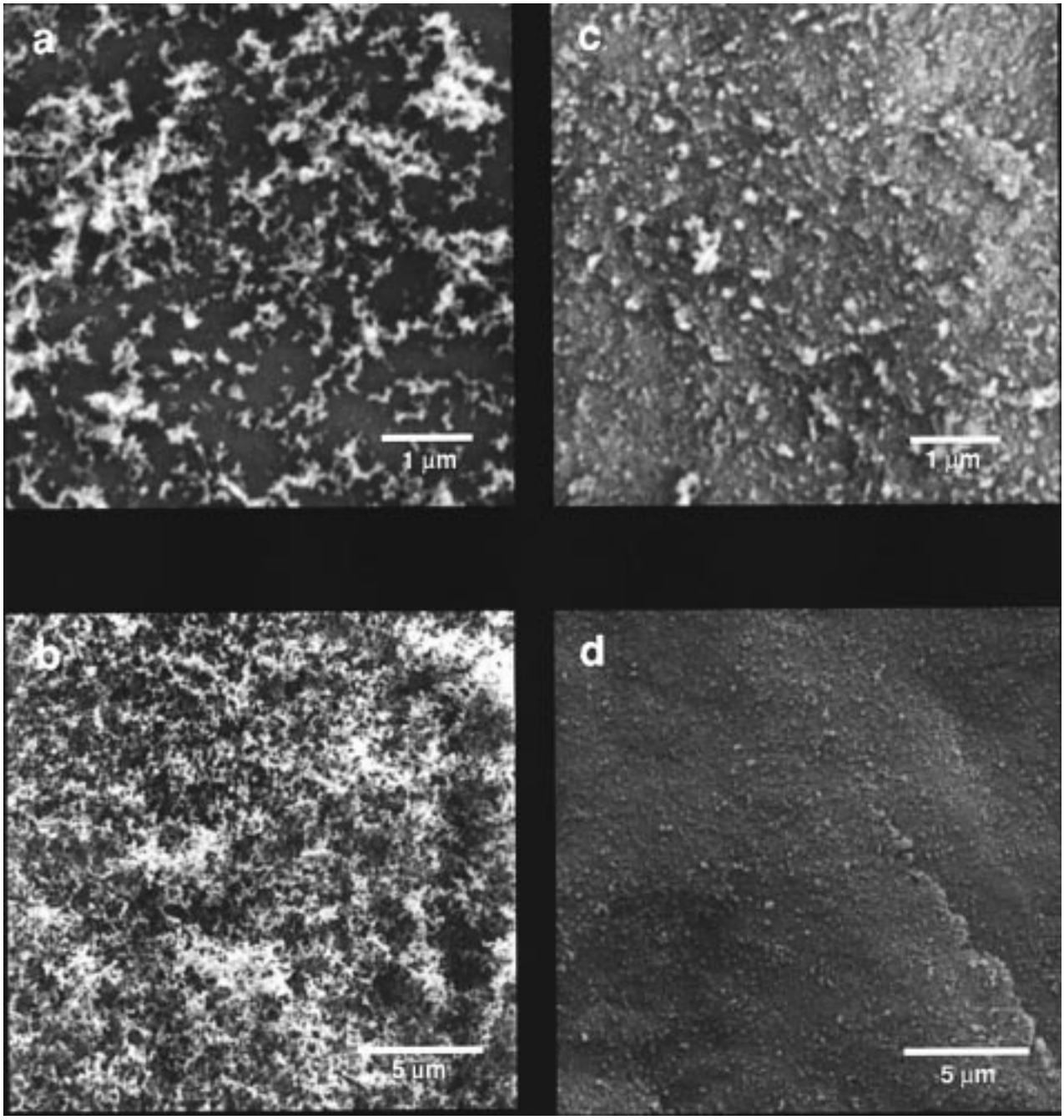

Figure 2. Scanning electron micrographics of flame-deposited kerosene soot on a silicon wafer chip (a and b) and a pressed chip of FW2 powder (c and d). Figure (a) was taken from a lightly deposited area on the silicon wafer in order to single out the image of individual soot particles, while figure (b) was taken from a heavily deposited area. Figures (c) and (d) were imaged from the same area of FW2 chip.

TABLE 1: Black Carbon Samples Used in HNO_3 Uptake Measurements

carbon sample	BET surface area (m^2/g)	the physical form of the carbon sample in the flow-tube reactor	sample mass in the flow tube
Degussa FW2	368	chips (irregular shape) or	3.1 g
		a pressed layer on a stainless steel plate	0.48 g
graphite	15	disk pellets or chips (irregular shape)	9.4 g (chips)
hexane soot	46	flame-deposited film on the flow-tube wall	58 mg
kerosene soot	91	flame-deposited film on a stainless steel plate	1−11 mg

was instead transformed into small chips having irregular shapes. Another sample for FW2 was prepared by pressing a layer of powder on a stainless steel plate (18 cm × 1.7 cm) in order to define a precise geometric surface area and was used for uptake coefficient measurements. Hexane and kerosene soot were directly flame-deposited on the reactor wall and a stainless steel plate (18 cm × 1.7 cm), respectively.

The morphology of the flame-deposited kerosene soot film and the pressed chip of FW2 was investigated by a scanning electron microscope (SEM, Camscan Series II). Their SEM images are shown in Figure 2. The kerosene soot film was deposited on a silicon wafer chip. The samples were gold-coated by using a gold sputter coater prior to the SEM analysis. Although the instrumental resolution was not high enough to

catch clear images of individual particles, the micrograph (Figure 2a) showed that the kerosene soot particles were highly aggregated into chain (or fractal) form with a typical individual particle size of ~0.1 μm or less. The size and morphology of the kerosene soot particles were quite similar to those of soot particles collected in the upper troposphere and lower stratosphere.[6] The kerosene soot film (Figure 2b) that was used for the uptake measurements showed very porous structure. The bulk density of the kerosene soot film was estimated by weighing the soot mass on a substrate with a known surface area and measuring the film thickness by SEM. The bulk density was found to be 0.038 g/cm^3 while the true density of soot was known to be in the range of 1.8−1.9 g/cm^3. The particles of FW2 were so small (d = 13 nm)[24] that they were not resolved at all in the SEM image. Unlike the kerosene soot film, the pressed chip of FW2 showed no porosity at the μm scale (Figure 2, parts c and d).

Every measurement of HNO_3 uptake was performed after baking the black carbon sample in the flow reactor under vacuum. Baking was done by wrapping a heating tape around the tubular reactor and leaving it for a few hours at 523 K. Samples were baked again after each measurement. No decrease in uptake coefficients or reactivity was observed over repeated uses. Thermal desorption studies were also carried out by heating the flow tube in the same way and monitoring the desorbing products mass-spectrometrically.

The detection of HNO_3 and its decomposition products were done by monitoring the mass signals (m/e) of 30 (NO^+), 46 (NO_2^+), and 63 (HNO_3^+). Since both HNO_3 and decomposition products gave mass 30 and 46 signals, the observed mass signals (S) were subtracted by the daughter ion signals of HNO_3 to give the decomposition product signals (S') by using the following equations:

$$S'_{30} = S_{30} - (S^\circ_{30}/S^\circ_{63})\, S_{63} \quad (2a)$$

$$S'_{46} = S_{46} - (S^\circ_{46}/S^\circ_{63})\, S_{63} \quad (2b)$$

where S° was the mass signal when HNO_3 was not exposed to soot.

The uptake coefficients of HNO_3 on black carbon surfaces were determined in a manner similar to our previous studies[25] and will be briefly described below. The mass signal, m/e 46, which had the highest intensity, was measured as a function of inlet position, z. The reaction time was calculated by using z/v, where v is the average flow velocity. Then the first-order rate constants, k, of HNO_3 uptake were obtained by plotting $\ln(S_{46}/S^\circ_{46})$ vs t. The axial gas-phase diffusion correction for k was made by using the following equation to give the corrected rate constant, k_g,

$$k_g = k\,(1 + kD/v^2) \quad (3)$$

where D, the diffusion coefficient of HNO_3 in He, was estimated to be pD = 495 Torr cm^2 s^{-1} at 296 K. A temperature dependence of $T^{1.76}$ for the diffusion coefficient was assumed for the estimation of D at 220 K. Since the symmetrical, cylindrical tube was not used for the uptake coefficients measurements, correction for radial gas-phase diffusion was not taken into account because this correction was considered to be imprecise. However, we estimated that it was less than 10%. The uptake coefficient, γ_g, was then calculated by using the following equation,

$$\gamma_g = 4k_gV/\omega S \quad (4)$$

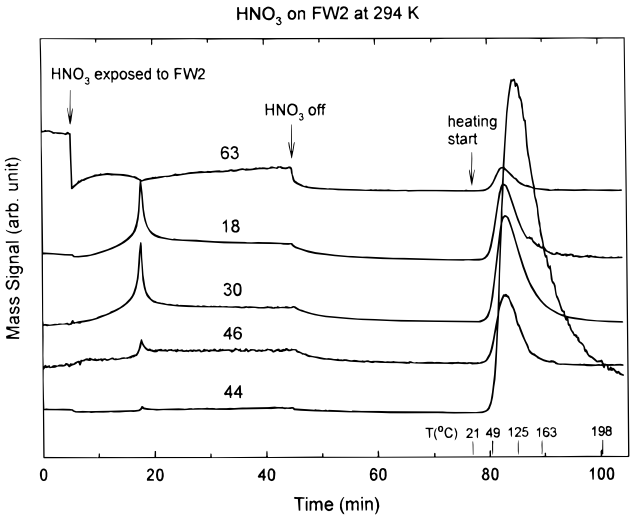

Figure 3. The uptake of HNO_3 on FW2 chips at 294 K and the subsequent thermal desorption. The experimental conditions are $P(HNO_3) = 4.3 \times 10^{-4}$ Torr, $P_t = 1.0$ Torr, $v = 935$ cm/s, $F_{HNO_3} = 3.8 \times 10^{16}$ molecules/s. The m/e 30 and 46 signals, which are calculated by using eq 2, directly represent the decomposition products of HNO_3 on soot surface. All the decomposition peaks of m/e 18, 30, 44, and 46 around 18 min are synchronous and are accompanied by a small dip in the m/e 63 signal.

where S is the geometric surface area of soot coated on the stainless steel plate, V the reactor volume, and ω the average molecular velocity of HNO_3.

Results and Discussion

HNO_3 + FW2. The uptake and decomposition of HNO_3 on FW2 chips under the conditions of $P(HNO_3) = 4.3 \times 10^{-4}$ Torr and T = 294 K are shown in Figure 3. The sliding injector of HNO_3 was placed at the downstream end of the flow reactor and then was moved upstream exposing FW2 surfaces. Mass signals of 18 (H_2O^+), 30 (NO^+), 44 (CO_2^+), 46 (NO_2^+), and 63 (HNO_3^+) were simultaneously monitored during the uptake and the following thermal desorption. Immediate uptake of HNO_3 was observed, and the subsequent appearance of product peaks of m/e 18, 30, 46, and 44 (very small) followed. The plotted mass 30 and 46 signals, which were subtracted by the daughter ion signals of parent HNO_3 molecules using eq 2, directly represented the actual decomposition products of HNO_3 molecules. All the decomposition peaks around 18 min were synchronous and accompanied by a small dip in the m/e 63 signal. The flow of HNO_3 was closed at 45 min, and then the heating of the flow tube was started at 78 min. Nitric acid molecules desorbed upon heating, but the total desorbed HNO_3 could account for only 10% of the total uptake. Water, CO_2, NO, and NO_2 desorbed as decomposition products from the heated surface along with HNO_3. However, the observed m/e 30 and 46 signals could not be fully ascribed to the decomposition products of NO and NO_2. In the presence of the decomposition products of NO and NO_2 only, the mass 30 signal should be greater than the mass 46 signal at least by 50%. However, the mass 30 signal was smaller than or about equal to the mass 46 signal in some parts during the experiment as shown in Figure 3. Unidentified decomposition/reaction products having m/e 30 or 46 fragment ions apparently desorbed along with NO and NO_2.

The occurrence of the HNO_3 decomposition peaks around 18 min in Figure 3 was further investigated by varying $P(HNO_3)$, and the results are presented in Figure 4. The appearance of

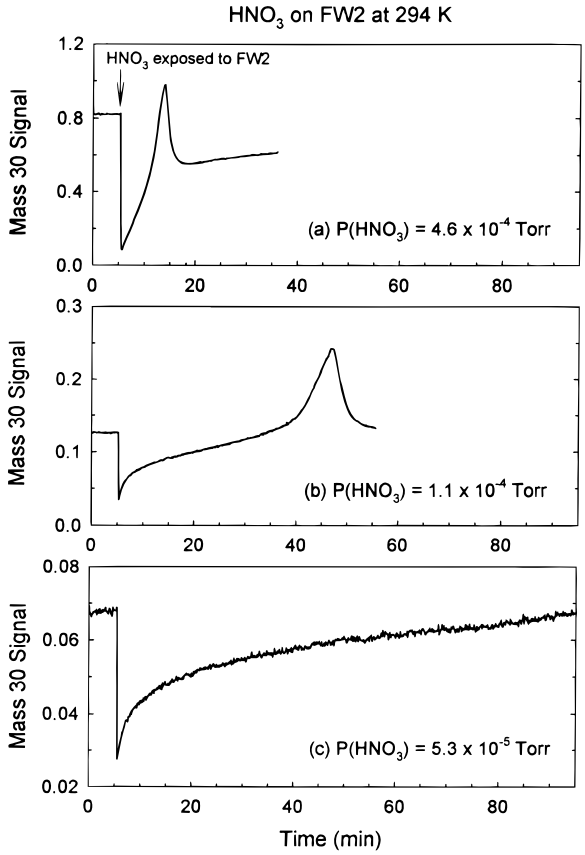

Figure 4. The appearance of the decomposition peaks at 294 K (shown in Figure 3) is found to be strongly dependent on the partial pressures of HNO_3. The appearance time of the *m*/*e* 30 peak is significantly delayed when the HNO_3 partial pressures lower from (a) 4.6×10^{-4} Torr to (b) 1.1×10^{-4} Torr. The peak does not appear at all at (c) $P(HNO_3) = 5.3 \times 10^{-5}$ Torr up to 90 min after soot exposure. The experimental conditions for each case are (a) $F_{HNO_3} = 4.1 \times 10^{16}$ molecules/s, $v = 943$ cm/s, $P_t = 1.0$ Torr, (b) $F_{HNO_3} = 3.0 \times 10^{16}$ molecules/s, $v = 2872$ cm/s, $P_t = 0.75$ Torr, and (c) $F_{HNO_3} = 1.4 \times 10^{16}$ molecules/s, $v = 2873$ cm/s, $P_t = 0.74$ Torr. The *m*/*e* 30 signal is the raw data which is not subtracted by the HNO_3 daughter ion signal.

the peak (monitored at *m*/*e* 30) was delayed from 8 min after soot exposure at $P(HNO_3) = 4.6 \times 10^{-4}$ Torr to 42 min at $P(HNO_3) = 1.1 \times 10^{-4}$ Torr and was never observed up to 90 min at $P(HNO_3) = 5.3 \times 10^{-5}$ Torr. On the other hand, the appearance of the decomposition peak was not observed at 223 K, even with $P(HNO_3) = 4.4 \times 10^{-4}$ Torr. It also critically depended on the conditions of the soot surface. When a HNO_3-uptake experiment was repeated under the same conditions as that of Figure 3, except that the soot sample was not baked in a vacuum after exposure to the atmosphere, the decomposition peak was not observed either. However, as long as the soot was sufficiently baked up to 523 K for a few hours in a vacuum after each experiment, the decomposition peak of HNO_3 was repeatedly observed with no sign of sample deterioration.

The observed pressure-dependence of HNO_3 decomposition on FW2 suggests that the decomposition is a bimolecular process operating at high surface coverage. To explain the behavior of HNO_3 decomposition on soot, the following mechanism is proposed as shown in Figure 5. As the surface coverage increases, two adsorbed HNO_3 molecules approach in close proximity. Bond breakage and rearrangement are then initiated on soot surfaces to form volatile products such as NO, NO_2, and H_2O. The soot surface reactivity in this step seems to be critically dependent on the surface temperature and the surface conditions (i.e., structure, composition, and cleanness) which were poorly defined in this study. As more surface sites become available with desorbing decomposition products, the second shallow dip in the HNO_3 uptake (Figure 3) is induced. After the initial decomposition of HNO_3, there remains an oxidized soot surface that is not active for further decomposition of HNO_3. Heating the oxidized soot surface gives off CO_2 as a product and restores the original surface. Due to the bimolecular nature of the above mechanism, the decomposition of HNO_3 occurred only at $P(HNO_3) > 10^{-4}$ Torr where the soot surface was saturated to a monolayer coverage (Figure 12a). Although the above-proposed mechanism seems to be oversimplified, it explains the main observed features of HNO_3 decomposition.

To see how HNO_3 interacts with soot under atmospheric conditions, the uptake and desorption behaviors of HNO_3 on FW2 at both 220 and 294 K were investigated under $P(HNO_3) = 5 \times 10^{-7}$ Torr (Figure 6). A pressed layer of FW2 on a stainless steel plate was used instead of irregularly shaped chips in order to define a geometric surface area of soot. The uptake of HNO_3 at 294 K quickly saturated and the subsequent desorption was reversible. No sign of HNO_3 decomposition was observed. The HNO_3 surface saturation concentration ($[HNO_3]_s$) at 294 K that was obtained by integrating the uptake area was 1.8×10^{15} molecules/cm^2 (based on the geometric area of the stainless steel plate). On the other hand, HNO_3 irreversibly condensed on FW2 at 220 K. Such condensation on the Pyrex reactor wall was not observed at the same temperature. Although the integrated HNO_3 uptake area at 220 K corresponded to a surface concentration greater than 7.2×10^{15} molecules/cm^2, which was at least four times $[HNO_3]_s$ at 294 K, it showed no sign of surface saturation. It is possible that multilayer adsorption occurs at 220 K.

Since it was not certain whether HNO_3 molecules were physically adsorbed or chemically dissociated on soot surfaces at 220 K, a thermal desorption experiment that was similar to one presented in Figure 3 was performed. The result is shown in Figure 7. At such a low concentration of HNO_3, only *m*/*e* 30 and 46 signals were measurable. The mass 30 and 46 signals plotted in Figure 7 were scaled to give the same intensity so that the two signals should fall on the same trace during the course of uptake and thermal desorption, unless HNO_3 decomposes. The deviation between two signals ($S_{30} > S_{46}$) at $T > 80$ °C indicated that adsorbed HNO_3 molecules started to decompose at this temperature. Possible decomposition products yielding the extra *m*/*e* 30 ion signal at $T > 80$ °C are either NO and NO_2 that originate from the destruction of HNO_3 or something else that originates from the reaction of HNO_3 with soot surface carbon. Judging from the fact that two mass signals coincided during the early stage of thermal desorption, no dissociated products seemed to be formed on FW2 at 220 K. Comparison of the uptake and desorption peak areas gave the desorption-to-uptake ratio of 1.1 for the mass 46 signal and 1.5 for the mass 30 signal.

The irreversible uptake of HNO_3 on FW2 at 220 K seems to be a result of some interactions (e.g., hydrogen bonding) between HNO_3 and surface functional groups. Soot is generally considered to have an aromatic surface structure covered with oxygen-containing functional groups—nearly every type of functional group known in organic chemistry has been proposed to be present on soot surfaces.[1b,2,13c] Semiquantitative energy-dispersive microanalysis using a scanning electron microscope (Camscan Series II) showed that both FW2 and kerosene soot contained a few percent of oxygen. In agreement with the above argument, we found that HNO_3 uptake/desorption on NaCl and

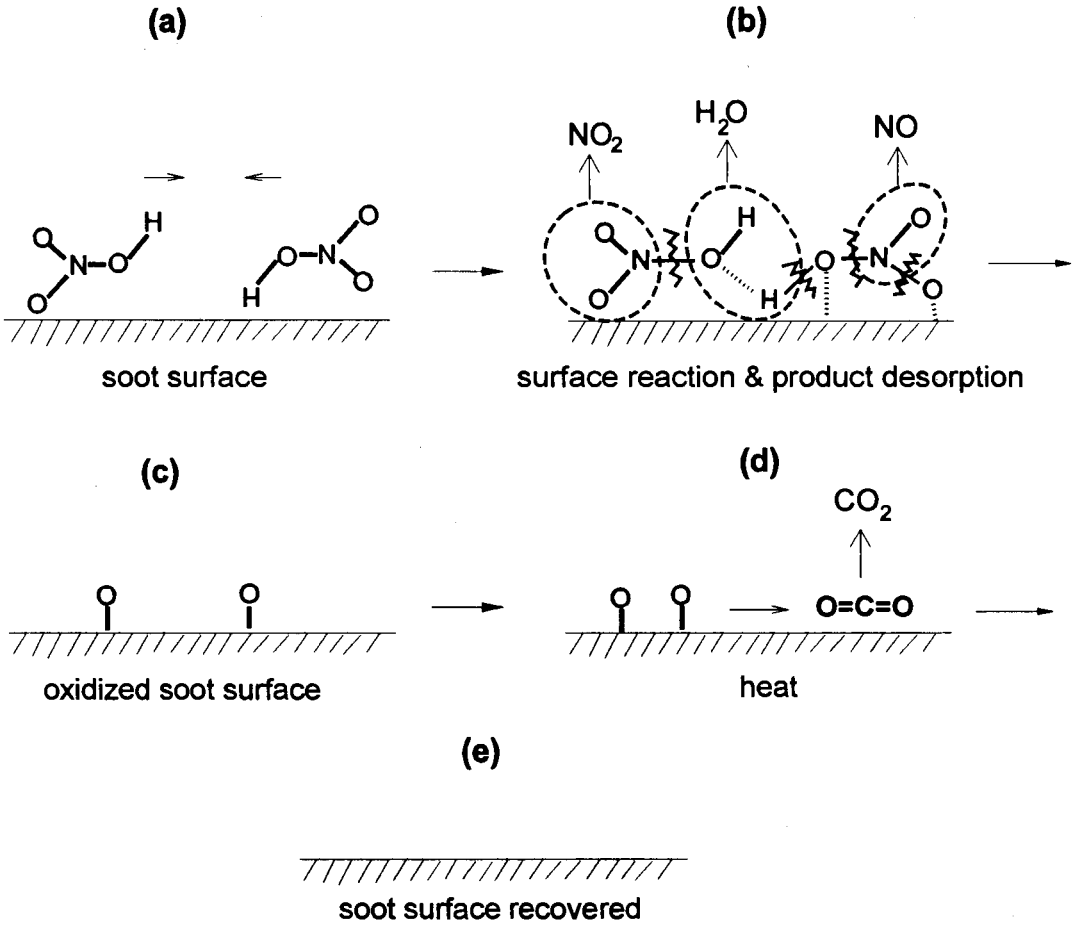

Figure 5. A proposed bimolecular mechanism of HNO_3 decomposition on soot at high surface concentrations.

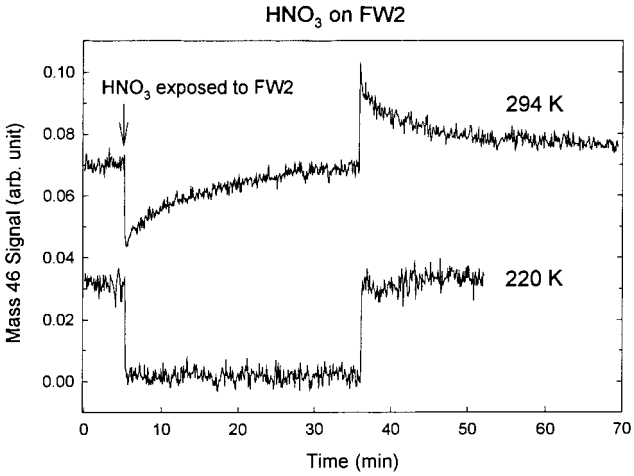

Figure 6. The uptake and desorption of HNO_3 on a pressed layer of FW2, which is supported on a stainless steel plate. The uptake starts when the HNO_3 inlet probe is pulled from downstream to upstream end (~5 min), and the desorption started when the probe is pushed back to the downstream end (~36 min). The uptake and desorption of HNO_3 are mainly reversible at 294 K, while those at 220 K are irreversible. The experimental conditions are $P(HNO_3) = 5 \times 10^{-7}$ Torr, $P_t = 0.37$ Torr, $v = 2064$ cm/s, $F_{HNO_3} = 8.4 \times 10^{13}$ molecules/s for the uptake at 294 K, and $P(HNO_3) = 5 \times 10^{-7}$ Torr, $P_t = 0.38$ Torr, $v = 1580$ cm/s, $F_{HNO_3} = 9.8 \times 10^{13}$ molecules/s for the uptake at 220 K. The data at 294 K are shifted upward for clarity.

$NaNO_3$, which did not have any surface functionality, was largely reversible at 223 K in our previous work.[25a]

While the adsorption of HNO_3 at low surface coverage was of largely physical nature at room temperature and below, HNO_3 immediately decomposed on a hot soot surface at a temperature of 503 K, as shown in Figure 8. Mass 30 and 46 signals were monitored while HNO_3 flowed through the heated reactor and then bypassed it. Upon exposure to soot the *m/e* 30 signal immediately increased, which implied an instant decomposition of HNO_3 to NO or NO_2. The result is consistent with that obtained by Thlibi and Petit.[19]

HNO_3 + Graphite. Graphite was chosen for this study as a reference black carbon sample since its structure and composition are relatively well-known, although most of carbon aerosols in the atmosphere are thought to be amorphous. Typical data collected at 295 K are shown in Figure 9. Nitric acid uptake on graphite pellets was as small as that on the Pyrex reactor wall. However, it should be noted that the uptake of HNO_3 on graphite pellets, although quite small, showed little sign of saturation in the time scale of a few minutes and that this small uptake was irreversible.

Since the reaction was relatively slow on graphite pellets, the external graphite surface area was increased by breaking the pellets into smaller chips. The reactivity study performed by using these chips is shown in Figure 10. Nitric acid was also found to decompose on graphite chips at 295 K, although the extent of decomposition was much smaller than that on FW2 (Figure 3). The mass 30 and 46 signals were modified according to eq 2 similar to those shown in Figure 3 to directly represent the decomposition products of HNO_3. Upon exposing HNO_3 to graphite, the mass 18 (water molecules) and 30 signals gradually increased while the mass 46 signal immediately rose above the mass 30 signal. Since S_{30} should always be higher than S_{46} with the presence of the decomposition products NO

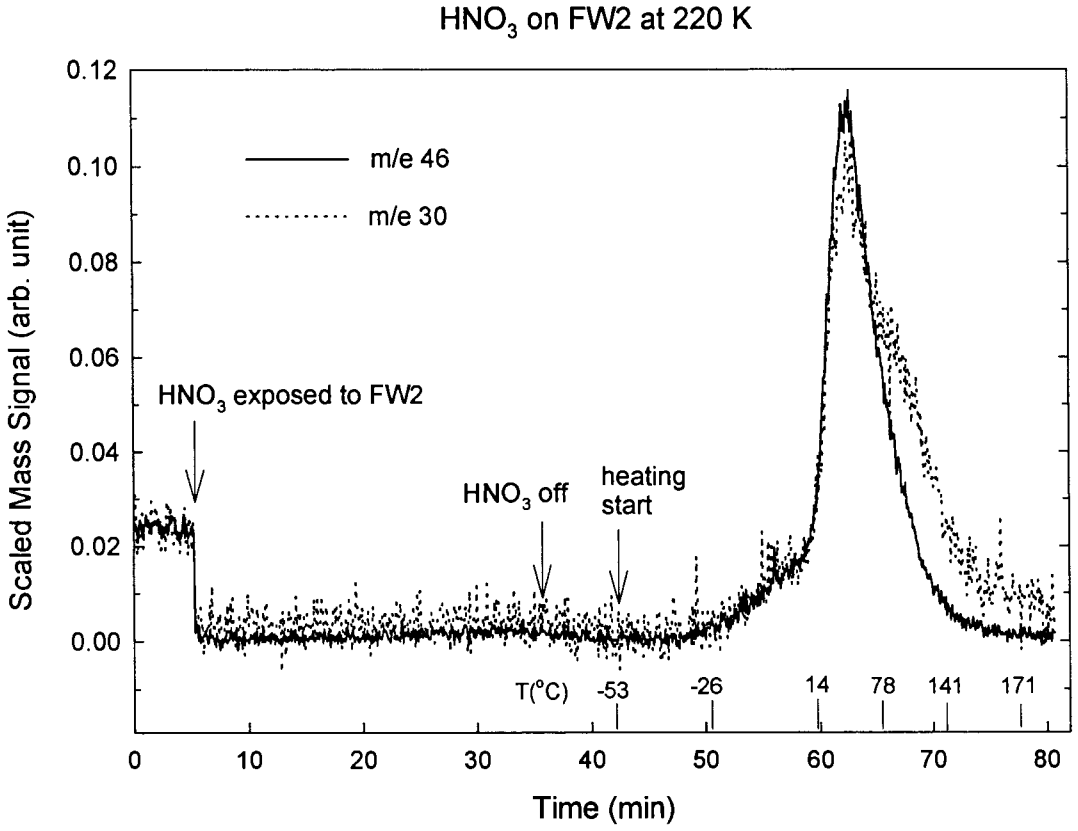

Figure 7. The uptake of HNO_3 on a pressed layer of FW2 at 220 K and the subsequent thermal desorption. The signals of mass 30 and 46 are scaled to give the same intensity. Without any decomposition of HNO_3 these signals are expected to fall on the same trace. The deviation of the two signals at $T > 80$ °C indicates that HNO_3 starts to decompose on FW2. The experimental conditions are $P(HNO_3) = 5 \times 10^{-7}$ Torr, $P_t = 0.35$ Torr, $v = 1659$ cm/s, and $F_{HNO_3} = 9.6 \times 10^{13}$ molecules/s.

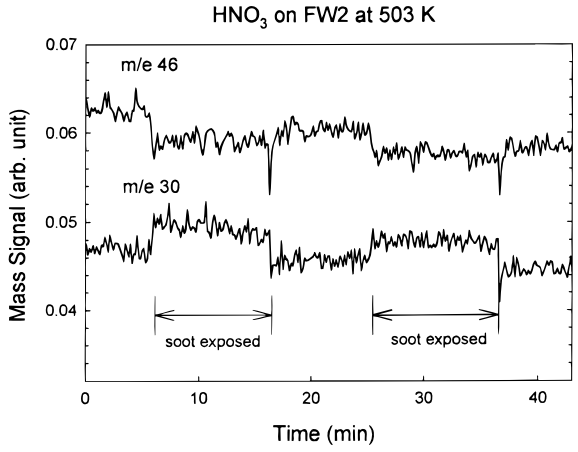

Figure 8. The decomposition of HNO_3 on FW2 chips at 503 K. Upon the exposure of HNO_3 to FW2, the mass 30 signal immediately increases, which suggests an instant decomposition of HNO_3. The experimental conditions are $P(HNO_3) = 2.1 \times 10^{-6}$ Torr, $P_t = 0.86$ Torr, and $v = 4230$ cm/s.

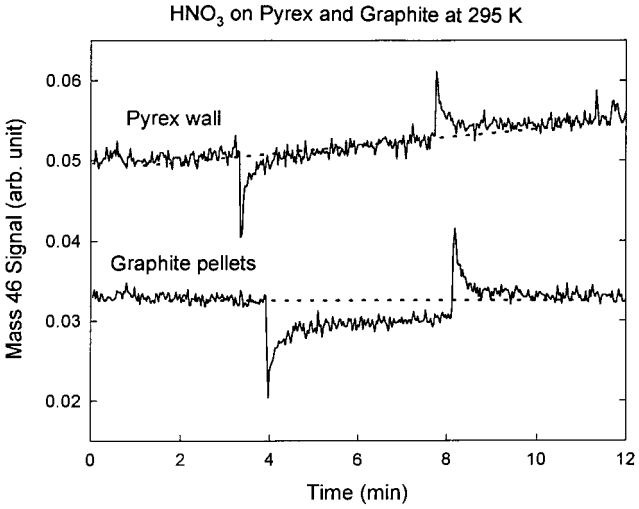

Figure 9. The uptake and desorption of HNO_3 on graphite pellets (7 pieces; each with a size of 1 in. diameter and a thickness of 1−2 mm) at 295 K are compared with those on a Pyrex surface. The experimental conditions in both cases are $P(HNO_3) = 4.1 \times 10^{-6}$ Torr, $P_t = 0.72$ Torr, $v = 970$ cm/s, and $F_{HNO_3} = 1.1 \times 10^{15}$ molecules/s. The data for Pyrex wall are shifted upward for clarity.

and NO_2, there seemed to be other unidentified decomposition products as in the case of FW2. The slight decrease of the mass 63 signal that was concurrent with the slowly rising decomposition product signals was reproducibly observed. All of these features were very similar to what was observed on FW2 in Figure 3. It is quite likely that the mechanism proposed in Figure 5 also works on graphite but with much less efficiency. As expected from the mechanism, the extent of HNO_3 decomposition got smaller with decreasing $P(HNO_3)$ and was negligible at $P(HNO_3) < 10^{-4}$ Torr. The huge mass 18 peak around 40 min resulted from the water desorption from the external probe surface when it was pushed into the vacuum from the atmosphere.

Graphite is known to react with concentrated aqueous nitric acid to form a graphite "oxide" that contains −C═O and −C−OH groups.[26] The reaction takes place not only on the outer surface but also between the graphite layers. A similar type of

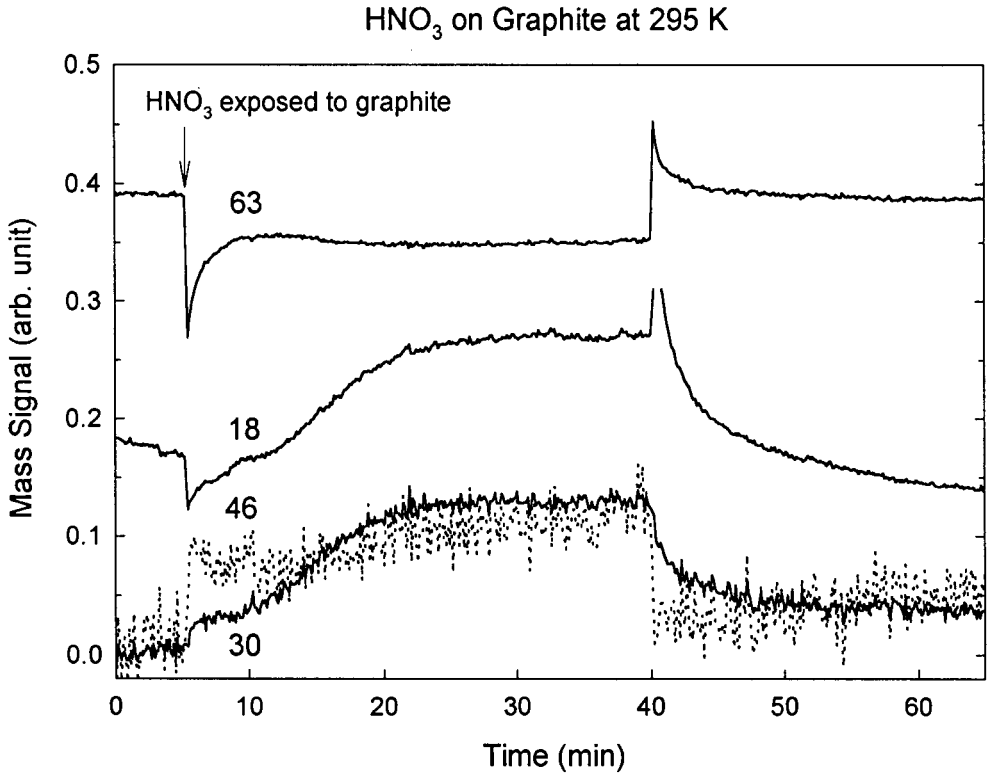

Figure 10. The uptake and desorption of HNO_3 on graphite chips at 295 K. The experimental conditions are $P(HNO_3) = 5.1 \times 10^{-4}$ Torr, $P_t = 1.0$ Torr, $v = 938$ cm/s, and $F_{HNO_3} = 4.6 \times 10^{16}$ molecules/s. The *m*/*e* 30 and 46 signals are calculated by using eq 2 to directly represent the decomposition products of HNO_3.

reaction is expected to take place at the gaseous HNO_3/graphite interface. Nitric acid molecules not only adsorb on the outer graphite plane but also penetrate between the layers. Since the spacing between two adjacent layers in graphite is 3.35 Å,[26] there is enough space for a planar HNO_3 molecule to be intercalated. The trapped HNO_3 molecules in the interlayer or interparticle space would react or diffuse out slowly. This may explain the irreversible uptake of HNO_3 on graphite pellets.

Graphite showed some reactivity for HNO_3 in this study and would form oxygen-containing surface functional groups on it as a result of the reaction. However, its uptake capacity and reactivity were much smaller than FW2. The relatively slow reactivity seems to be mainly due to the lack of surface functionality for graphite, which may play a significant role in determining the reactivity of black carbon. The relationship between the structure and reactivity of soot needs to be further investigated in the laboratory.

HNO_3 + Hexane Soot. The uptake and desorption of HNO_3 on flame-deposited hexane soot film were also investigated. Typical data at 295 K are shown in Figure 11. The deposited soot mass was 58 mg. The geometric and B.E.T. surface area of soot were measured and found to be 177 cm^2 and 2.65 m^2, respectively. If the bulk density of hexane soot film is assumed to be equal to that of kerosene soot ($\rho_{bulk} = 0.038$ g/cm^3), the deposited film thickness is estimated to be about 86 μm, which corresponds to about 1200 particle layers. In Figure 11 the mass signals of 30, 46, and 63 were simultaneously monitored during the course of the uptake and the following desorption at $P(HNO_3) = 3.1 \times 10^{-5}$ Torr and 4.0×10^{-4} Torr. The signals of *m*/*e* 30 and 46 were scaled to give the same intensity to the *m*/*e* 63 signal and were shifted upward in order to avoid overlapping. Without HNO_3 decomposition on soot, the signals of *m*/*e* 30, 46, and 63 should follow the same trajectories during the course of uptake and desorption. These are exactly the results shown in Figure 11. The observation clearly suggests that the interaction of HNO_3/hexane soot is mainly physical adsorption.

The above-mentioned results suggest that hexane soot is less reactive for HNO_3 than graphite, although the former has more surface functionalities than the latter. However, the observed reactivities among different carbon samples in this study are not directly comparable because the total reactive surface area involved in each sample is quite different. For example, the total surface area of the hexane soot film is 2.65 m^2 while that of graphite chips is much larger, 141 m^2 (Table 1). As mentioned earlier in the Experimental Section, both the graphite chip and the graphite powder have the same specific B.E.T. surface area. Even if only 10% of the total graphite chip surface is available, it is still five times larger than the total hexane soot surface. Therefore, it should not be concluded from the present results that hexane soot is nonreactive or less reactive for HNO_3 than graphite.

A series of HNO_3 uptake experiments on hexane soot at 295 K was performed by varying the partial pressure of HNO_3, and then the adsorbed amounts of HNO_3 were calculated by integrating the uptake peak area. An adsorption isotherm of HNO_3 on hexane soot, which is shown in Figure 12a, was obtained by plotting the adsorbed amount of HNO_3 as a function of $P(HNO_3)$. The results suggested that it followed a typical behavior of adsorption isotherm. The soot surface was rapidly saturated with increasing HNO_3 partial pressure at $P(HNO_3) < 1 \times 10^{-4}$ Torr, reached a monolayer coverage around $P(HNO_3) = 2 \times 10^{-4}$ Torr, and started to show multilayer adsorption at $P(HNO_3) > 2 \times 10^{-4}$ Torr. The first four data points in the lower $P(HNO_3)$ were fitted to the Langmuir adsorption isotherm (eq 5)[27] as shown in Figure 12b:

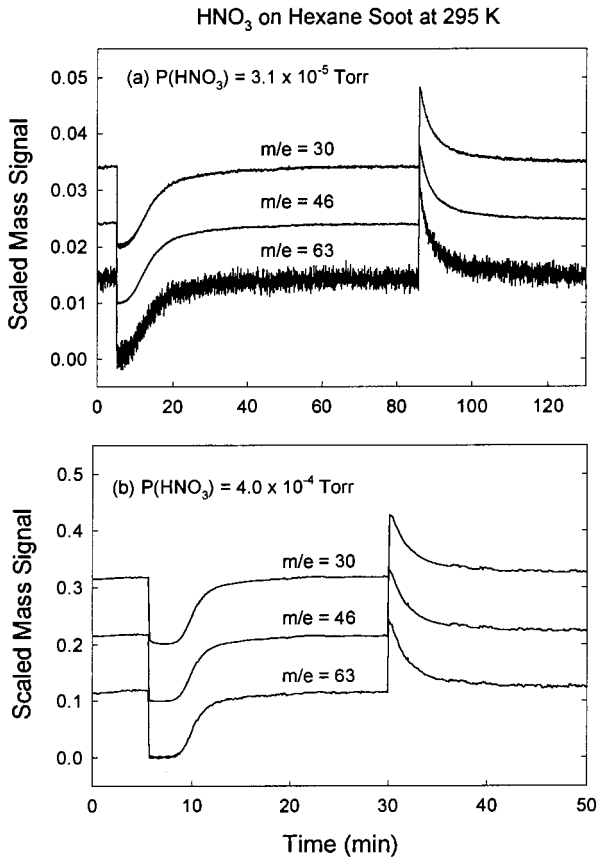

Figure 11. The uptake and desorption of HNO_3 on flame-deposited hexane soot at 295 K. The mainly reversible uptake and desorption behaviors are demonstrated at two different HNO_3 partial pressures of (a) 3.1×10^{-5} Torr and (b) 4.0×10^{-4} Torr. The experimental conditions for each case are (a) $P_t = 0.89$ Torr, $v = 1758$ cm/s, $F_{HNO_3} = 9.6 \times 10^{15}$ molecules/s, and (b) $P_t = 0.94$ Torr, $v = 641$ cm/s, $F_{HNO_3} = 4.5 \times 10^{16}$ molecules/s.

$$\frac{P(\mathrm{HNO_3})}{V_{ad}} = \frac{1}{V_{mono}} P(\mathrm{HNO_3}) + \frac{1}{K_{ad} V_{mono}} \qquad (5)$$

where V_{mono} is the HNO_3 volume at STP corresponding to monolayer coverage and K_{ad} is the Langmuir adsorption constant of the HNO_3/hexane soot system. The values of $V_{mono} = 0.37$ cm^3 and $K_{ad} = 5.4 \times 10^4$ $Torr^{-1}$ were obtained from the slope and intercept of the straight line shown in Figure 12b. It should be noted that the reported values of K_{ad} for the adsorption of nitrous oxide, ethylene, and nitrogen on charcoal surface at 293 K were all in the range of 10^{-3} to 10^{-4} $Torr^{-1}$,[28] much smaller than present value of K_{ad} for the HNO_3/hexane soot system. The extreme stickiness of the HNO_3 molecule could be ascribed to the formation of hydrogen bonding on the soot surface.

The monolayer surface concentration of HNO_3 obtained from V_{mono} and soot surface area is 5.6×10^{16} or 3.8×10^{14} molecules/cm^2 on the basis of the geometric or B.E.T. surface area, respectively. The average cross section (σ_{HNO_3}) of an adsorbed HNO_3 molecule using the B.E.T. surface area is 26.3 $Å^2$ while σ_{HNO3} based on the geometric surface area of the reactor is only 0.18 $Å^2$ which is considered to be unreasonably small. It should be noted that the value of σ_{N_2} that is commonly used for the B.E.T. surface area measurements is 16.2 $Å^2$. Thus, a value of $\sigma_{HNO_3} = 26.3$ $Å^2$ using the B.E.T. surface area seems to be much more reasonable. This implies that the adsorption of HNO_3 on soot film at saturation is accessible to the underlying carbon layers, not just limited to the top layers.

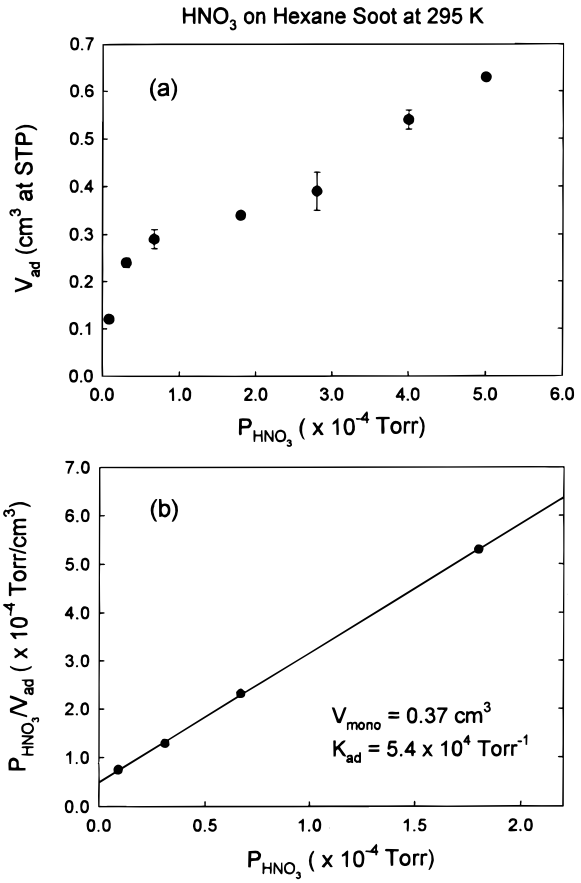

Figure 12. (a) The HNO_3 adsorption isotherm on hexane soot which is obtained by plotting the adsorbed amount of HNO_3 as a function of $P(HNO_3)$ and (b) the fit to the Langmuir adsorption isotherm (eq 5) for the four data points at lower HNO_3 pressures. Experimental conditions are similar to those given in Figure 11.

HNO_3 + Kerosene Soot. Kerosene soot was flame-deposited on a stainless steel plate ($S_g = 31.6$ cm^2) and the deposited soot mass was found to be 10.9 mg. The B.E.T. surface area of soot was also measured and found to be 0.99 m^2. A rough estimate gave about 2500 particle layers for the soot film on the basis of the measured bulk density (0.038 g/cm^3) and the B.E.T. surface area. The kerosene soot is expected to have composition and structure similar to those of hexane soot because they were prepared in the same way under identical combustion conditions. Therefore, their reactivities would be similar. The uptake and desorption of HNO_3 on kerosene soot at 295 K were largely reversible at both $P(HNO_3) = 2.1 \times 10^{-4}$ and 6×10^{-7} Torr (Figure 13). No sign of decomposition of HNO_3 was observed even at $P(HNO_3) > 10^{-4}$ Torr. A similar thermal desorption experiment shown in Figure 7 was also performed for kerosene soot. The result is presented in Figure 14. The uptake of HNO_3 on kerosene soot at 219 K was found to be irreversible. The plotted mass 30 and 46 signals were scaled to give the same intensity as in Figure 7. Unlike the case of FW2 (Figure 7) where the deviation started at $T >$ 80 °C, the deviation between the two signals occurred around $T = 50$ °C (the center of the desorption peak). Although the origin of the extra mass 46 signal in this region was not understood, it surely indicated that volatile decomposition products, which were not NO or NO_2, desorbed from the soot surface. Comparison of the uptake and desorption peak areas gave the desorption-to-uptake ratio of 1.1 for mass 46 and 0.9 for mass 30.

Uptake Coefficients of HNO_3 on Soot. A typical first-order plot of HNO_3 signal loss on soot surfaces as a function of

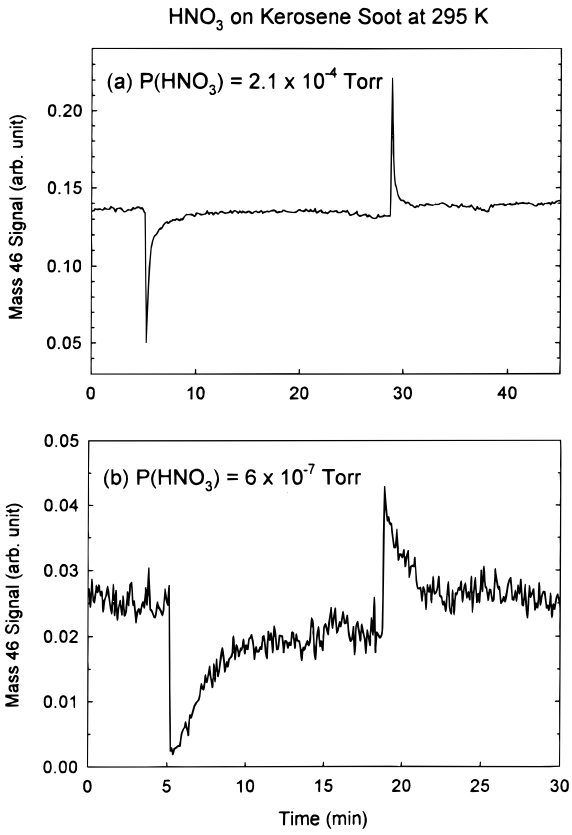

Figure 13. The uptake and desorption of HNO_3 on flame-deposited kerosene soot at 295 K at (a) $P(HNO_3) = 2.1 \times 10^{-4}$ Torr and (b) $P(HNO_3) = 6 \times 10^{-7}$ Torr. The experimental conditions for each case are (a) $P_t = 0.38$ Torr, $v = 2152$ cm/s, $F_{HNO_3} = 3.9 \times 10^{16}$ molecules/s, and (b) $P_t = 0.37$ Torr, $v = 2150$ cm/s, $F_{HNO_3} = 1.0 \times 10^{14}$ molecules/s.

TABLE 2: Summary of HNO_3 Uptake Coefficient Measurements[a]

	γ_g	
	295 (±1) K	220 (±1) K
kerosene soot[b]	0.060 (±0.005)[c]	0.093 (±0.002)
hexane soot[d]	0.023 (±0.004)	
Degussa FW2[e]	0.067 (±0.005)	0.13 (±0.01)

[a] All measurements except for hexane soot were performed at the conditions of $P(HNO_3) = 5 \times 10^{-7}$ Torr and $P_t = 0.37$ Torr The experimental conditions for hexane soot were $P(HNO_3) = 2 \times 10^{-6}$ Torr and $P_t = 0.88$ Torr. [b] A flame-deposited soot film on a stainless steel plate. [c] The error limit indicates one standard deviation from eight or nine measurements. [d] A flame-deposited soot film on cylindrical Pyrex reactor wall. [e] A pressed layer of powder on a stainless steel plate.

reaction time (i.e., the injector position) is shown in Figure 15. From the slope of this plot the γ_g was determined by using eqs 3 and 4. The results for kerosene soot, hexane soot, and FW2 are summarized in Table 2. FW2 gave slightly higher γ_g value than the kerosene soot. The γ_g increased by 55% for kerosene soot and by 94% for FW2 when the temperature dropped from 295 to 220 K. The observation is consistent with the typical behavior of the physical adsorption process. The γ_g on hexane soot at 295 K was also measured to be 0.023 (±0.004). The uptake coefficient of HNO_3 on graphite pellets was as small as that on Pyrex (Figure 9) and was not determined. The varying γ_g values over different kinds of soot samples could be also ascribed to differences in the density of surface functionalities and morphology of soot substrates.

The uptake coefficients measured in this work showed a strong time dependence in some cases due to the surface saturation (or deactivation) effect. In Figure 16 the HNO_3 uptake coefficients on FW2 at 220 and 295 K are plotted as a function of the exposure time. The γ_g at 295 K rapidly decreased from its initial value to a negligible value within 30 min even under $P(HNO_3) = 5 \times 10^{-7}$ Torr, while γ_g at 220 K showed only a slight decrease at the same time scale. Strong time-dependent behaviors of γ_g were also observed with other black carbons at room temperature. The γ_g values listed in Table 2 are the initial values measured at shorter time scale.

It should be kept in mind that the γ_g values listed in Table 2 are all based on the geometric area of the reactor covered with soot. Recently Keyser et al.[29] have suggested that the internal surface area must be taken into account in determining the true uptake coefficient (γ_t) if the morphology of substrates is measured. While the pressed FW2 showed little porosity in the SEM images of Figure 2, kerosene soot film exhibited a highly porous structure which contained a large internal surface area. Considering this internal surface area, the true uptake coefficient (γ_t) of HNO_3 on kerosene soot would be much smaller than the listed γ_g while γ_g for FW2 substrate seems to be a pretty good approximation of γ_t.

To investigate the effect of the internal surface area on the uptake coefficient measurements, γ_g was measured by varying the total deposited mass of kerosene soot (i.e., the total surface area) on the same geometric substrate area. The total B.E.T. surface area of the deposited soot was found to be directly proportional to the soot mass from 1 to 11 mg. The estimated numbers of soot particle layers are 230 for 1 mg of soot mass and 2500 for 11 mg of soot on the basis of the measured bulk density and BET surface area. The results are plotted in Figure 17 where γ_g showed little dependence (~20%) on the internal surface area. This is not unexpected because of the very large layers of packing in the substrate used. It is further noted that the morphology of the kerosene soot as shown in Figure 2 is not simply packed (i.e., either hexagonal close packing or simple cubic packing) which may be required in the theoretical model.

In a similar study, Fenter et al.[30] measured the reactive uptake coefficient of HNO_3 on NaCl or KBr grains as a function of the salt grain layer (1−10 layers) and found no mass dependence while the model calculation according to Keyser et al.[29] predicted it. They ascribed this mass independence of γ to the *sticky* nature of HNO_3. The sticky collision of a HNO_3 molecule, which means a nonnegligible residence time on the surface, makes the HNO_3 diffusion into the internal surface much slower than predicted by the diffusion model and prevents the HNO_3 molecule from reaching the underlying layers. The same argument could be applied to the present HNO_3/soot system. If the stickiness keeps the HNO_3 molecules within the top few layers, the increase of the underlying soot layers has little effect on γ. However, if sufficient time is allowed to reach an equilibrium saturation, the internal soot surface would be eventually available for HNO_3 uptake as mentioned earlier. Unfortunately, their study was performed using rather large HNO_3 concentrations, about 2 or 3 orders of magnitude greater than the work in the present study. As discussed in the previous sections, the uptake mechanisms may change from high concentrations to low concentrations.

Effect of Concentrated H_2SO_4-coating on Soot Surface. The possible role of aqueous acid chemistry in decomposing HNO_3 to NO_x in the presence of soot should be also considered since many soot particles found in the lower stratosphere are incorporated in sulfuric acid aerosols. Nitric acid is known to

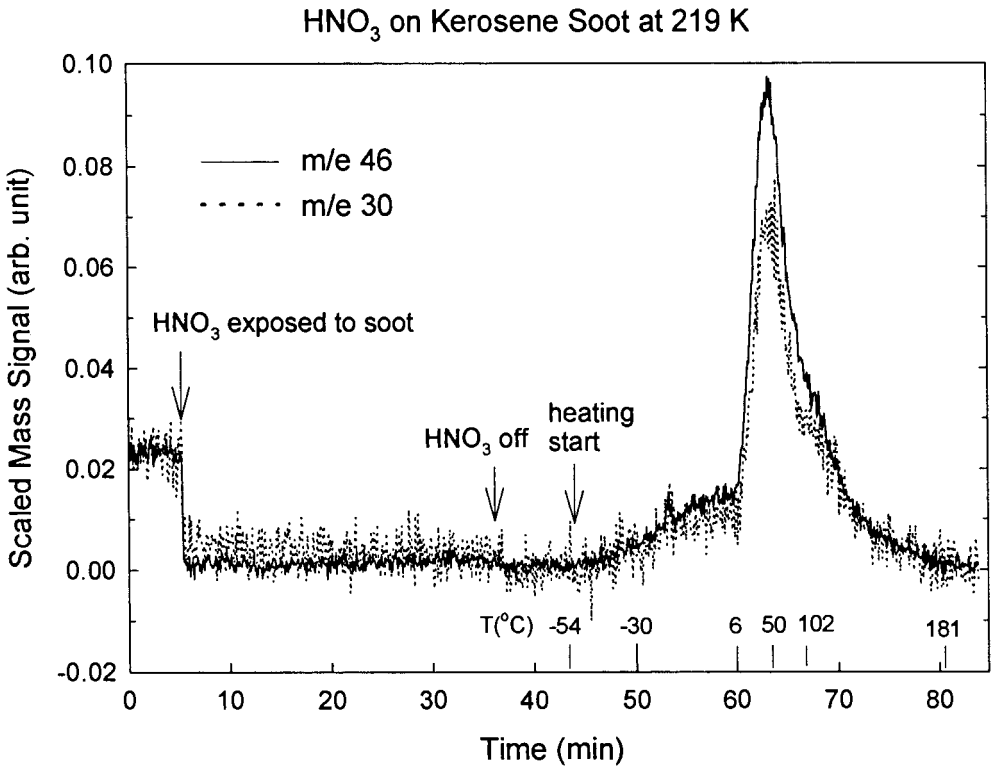

Figure 14. The uptake of HNO_3 on kerosene soot at 219 K and the subsequent thermal desorption. The signals of mass 30 and 46 are scaled to give the same intensity as in Figure 7. The experimental conditions are $P(HNO_3) = 5 \times 10^{-7}$ Torr, $P_t = 0.35$ Torr, $v = 1662$ cm/s, and $F_{HNO_3} = 9.8 \times 10^{13}$ molecules/s.

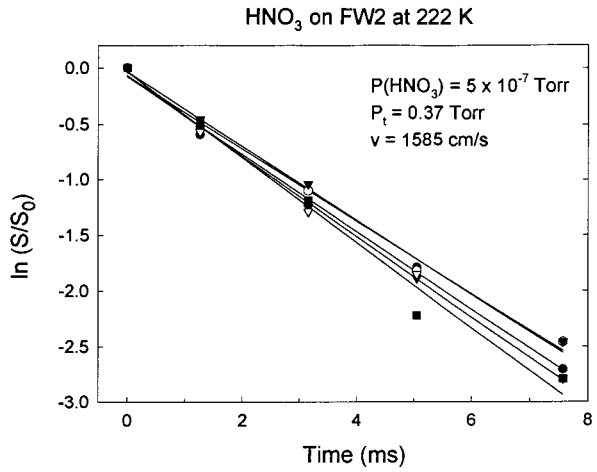

Figure 15. A typical first-order plot of loss of HNO_3 signals as a function of the reaction time (i.e., movable inlet position) on a pressed layer of FW2 at 222 K. The experimental conditions are $P(HNO_3) = 5 \times 10^{-7}$ Torr, $P_t = 0.37$ Torr, $v = 1585$ cm/s, and $S_g = 23.4$ cm^2. The different symbols represent the repetition of the measurements under the same conditions.

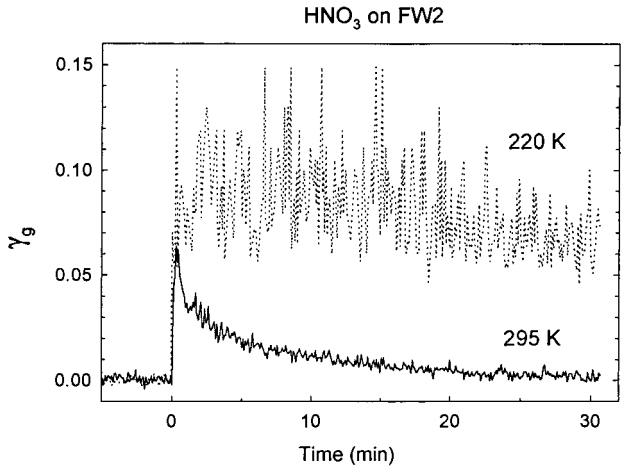

Figure 16. The time-dependent HNO_3 uptake coefficients measured on a pressed FW2 layer at 220 and 295 K are compared. The partial pressure of HNO_3 and the total pressure in the flow tube are 5×10^{-7} Torr and 0.37 Torr, respectively.

dissociate to give nitronium ion (NO_2^+) in strong acid (reaction 6).[26] The nitronium ion may take part in a redox reaction (reaction 7) on soot surfaces to produce NO and/or NO_2, which would be subsequently volatilized out of the aqueous phase due to its low Henry's law constant.

$$HNO_3 + H_2SO_4 \leftrightarrow NO_2^+ + HSO_4^- + H_2O \qquad (6)$$

$$NO_2^+ + \text{soot} \rightarrow NO_2 + \text{soot (oxidized)} \qquad (7)$$

One set of data is shown in Figure 18. We coated concentrated sulfuric acid (>90 wt %) on hexane soot at 296 K. The mass 46 signals clearly show irreversible uptake while the mass 30 signal evolved from soot surfaces. The results strongly support the proposed mechanism.

We also performed a series of experiments by coating 120 mg of concentrated sulfuric acid (>90 wt %) on an FW2 surface at 296 K under similar experimental conditions. The mass of FW2 substrate was also measured to be about 0.5 g. Again, the pronounced formation of the mass 30 signals during the uptake of HNO_3 occurred. However, when the temperature of the reactor dropped to around 230 K, we found that the uptake/desorption peaks are reversible It appears that reaction 6 proceeded very slowly at low temperature and the mechanism shifted from the reactive uptake to the physical uptake. Furthermore, the results for experiments using sulfuric acid of

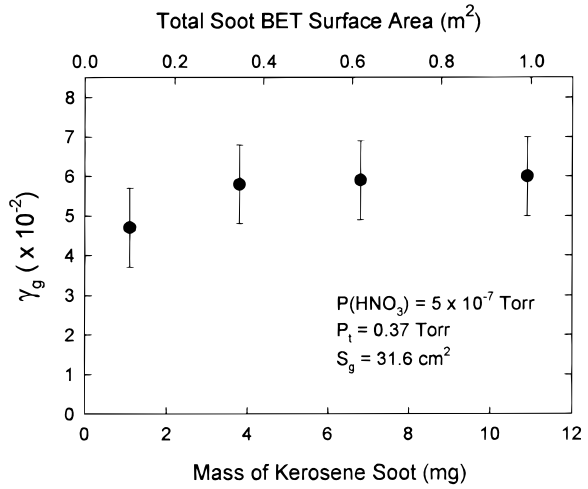

Figure 17. The dependence of HNO_3 uptake coefficient (γ_g) at 295 K on the mass of flame-deposited kerosene soot. The total BET surface area of the deposited kerosene soot is measured to be directly proportional to the soot mass. The experimental conditions are $P(HNO_3) = 5 \times 10^{-7}$ Torr, $P_t = 0.37$ Torr, $\nu = 2090$ to 2150 cm/s, and $S_g = 31.6$ cm^2.

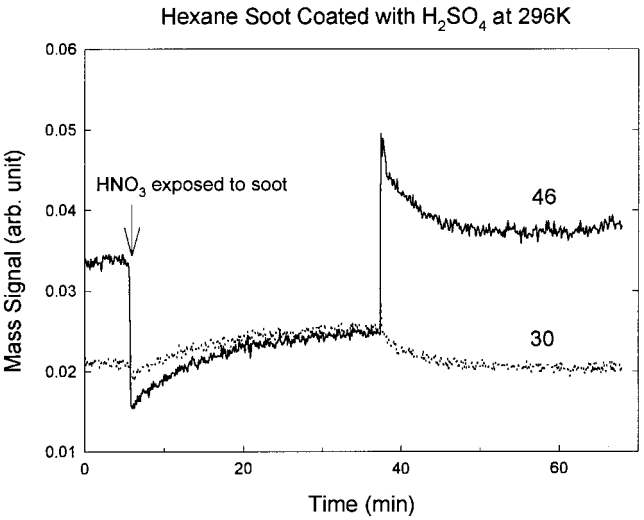

Figure 18. The uptake of HNO_3 on hexane soot coated with sulfuric acid at 296 K. The experimental conditions are $P(HNO_3) = 5.3 \times 10^{-6}$ Torr, $P_t = 0.875$ Torr, $\nu = 1738$ cm/s, $m(H_2SO_4) = 20$ mg, and m(soot) = 58 mg. Significant NO evolved during the uptake of HNO_3.

60−70 wt % also suggest the physical uptake of HNO_3.[31] This observation has significant implications for atmospheric chemistry as discussed below.

Atmospheric Implications. Since almost any heterogeneous surface reaction shows a strong dependence of its reactivity on the choice of the solid substrates, it is essential to have a well-defined surface for better understanding of the reaction. However, soot is a very poorly understood material which does not have any uniquely defined structure. The structure and property of soot vary greatly depending on its carbonaceous starting materials and its combustion conditions. Therefore, atmospheric carbon aerosols cannot be truly represented by any single black carbon material. Nevertheless, the present study that used four different black carbon samples may provide useful information for assessing the role of carbon aerosols in the heterogeneous chemistry of HNO_3 in the atmosphere.

Although each black carbon sample displayed different reactivity for HNO_3, they all showed little sign of reactivity under the atmospheric conditions of $P(HNO_3) \sim 10^{-7}$ Torr and $T \sim 220$ K. Nitric acid molecules simply physisorbed on soot surfaces until the surfaces were saturated to a monolayer coverage at $P(HNO_3) \geq 10^{-4}$ Torr. Since such a high concentration of HNO_3 does not exist in the upper atmosphere, the HNO_3 coverage on soot aerosols is always far below the monolayer saturation. In addition, it should also be considered that some of the soot samples used in this study were baked in a vacuum prior to each uptake measurement. Otherwise, they showed little reactivity perhaps due to the presence of water on soot surfaces. The black carbon used in this study intends to mimic the atmospheric soot aerosols which are always covered with a thin layer of water and/or sulfuric acid to some extent.

Another interesting aspect is the high-temperature reactivity of soot for HNO_3 (Figure 8). The high-temperature reactivity does not have significant atmospheric implication, but it may have some effect in the jet and dispersion of aircraft plumes. Thlibi and Petit[19] addressed a similar issue related to NO destruction in the jet regime and estimated this effect to be negligible. The destruction of HNO_3 in the jet regime, if any, seems to be too transient and localized to have a major atmospheric impact.

Recently, Chatfield[32] and Jayne et al.[33] have suggested a renoxification mechanism that the aqueous-phase reaction of HNO_3 and HCHO in aerosols or cloud droplets produce HONO or NO and NO_2. A kinetic and mechanistic study of this redox reaction has been reported by Horváth et al.[34] Since various carbonyl and aldehyde groups could exist on soot surface in aircraft plumes, the heterogeneous counterpart of homogeneous HNO_3 + HCHO reaction in liquid phase may proceed on soot to produce similar products. But, it should be noted that the concentrations of HCHO in the upper troposphere and lower stratosphere are very small, possibly in the ppt range. We do not expect it will play a major role in atmospheric chemistry.

The overall results of this work suggest that the direct reactivity of black carbons for HNO_3, if any, is not important under the atmospheric conditions of upper troposphere and lower stratosphere. However, the conclusion should not be definitive unless the real soot aerosol materials about which we have little information are tested. To get more conclusive answers, future research should be directed for characterizing atmospheric soot aerosol samples and understanding their heterogeneous chemistry.

Conclusions

In the present work we investigated the chemical and physical interactions of HNO_3 with black carbon under various conditions. Under the condition of $P(HNO_3) \geq 10^{-4}$ Torr and room-temperature HNO_3 decomposed to give NO_x and H_2O as main products on black carbon FW2. A bimolecular decomposition mechanism on the soot surface has been proposed in order to explain the observed facts. However, the mechanism seems not to work at much lower surface coverage. Graphite showed a similar but much lower reactivity for HNO_3 than FW2. Hexane and kerosene soot showed little sign of reactivity for HNO_3. It is rather difficult to directly compare reactivity over different black carbon samples, because a wide range of total surface area associated with different physical forms was employed in the HNO_3 uptake measurement. However, all black carbon samples tested in this study showed no reactivity for HNO_3 either at $P(HNO_3) = 5 \times 10^{-7}$ Torr or at $T = 220$ K where nitric acid was found to physically adsorb with its γ_g value in the range of 10^{-2} to 10^{-1}. Judging from this fact, it seems to be very unlikely that HNO_3 is reduced to NO_x on aircraft-generated soot aerosols in the upper troposphere and lower stratosphere.

Acknowledgment. The research was performed at the Jet Propulsion Laboratory, California Institute of Technology, under a contract with the National Aeronautics and Space Administration (NASA). We thank our colleagues Leon Keyser, Francois Caloz, Ross Salawitch, and Yuk Yung for fruitful discussions.

References and Notes

(1) (a) *Soot Formation in Combustion—Mechanisms and Models*; Bockhorn, H., Ed.; Springer-Verlag: Berlin, 1994. (b) Mattson, J. S.; Mark, H. B., Jr. *Activated Carbon: Surface Chemistry and Adsorption from Solution*; Marcel Dekker: New York, 1971.

(2) Goldberg, E. D. *Black Carbon in the Environment: Properties and Distribution*; Wiley-Interscience: New York, 1985.

(3) Penner, J. E.; Novakov, T. *J. Geophys. Res.* **1996**, *101*, 19373.

(4) Cooke, W. F.; Wilson, J. J. N. *J. Geophys. Res.* **1996**, *101*, 19395.

(5) Pusechel, R. F.; Blake, D. F.; Snetsinger, K. G.; Hansen, A. D. A.; Verma, S.; Kato, K. *Geophys. Res. Lett.* **1992**, *19*, 1659.

(6) Blake, D. F.; Kato, K. *J. Geophys. Res.* **1995**, *100*, 7195.

(7) Horvath, H. *Atmos. Environ.* **1993**, *27A*, 293.

(8) Jensen, E. J.; Toon, O. B. *Geophys. Res. Lett.* **1997**, *24*, 249.

(9) Novakov, T.; Chang, S. G.; Harker, A. B. *Science* **1974**, *186*, 259.

(10) Baldwin, A. C. *Int. J. Chem. Kinet.* **1982**, *14*, 269.

(11) Stephens, S.; Rossi, M. J.; Golden, D. M. *Int. J. Chem. Kinet.* **1986**, *18*, 1133.

(12) Smith, D. M.; Chughtai, A. R. *J. Geophys. Res.* **1996**, *101*, 19607.

(13) (a) Akhter, M. S.; Chughtai, A. R.; Smith, D. M. *J. Phys. Chem.* **1984**, *88*, 5334. (b) Chughtai, A. R.; Gordon, S. A.; Smith, D. M. *Carbon* **1994**, *32*, 405. (c) Smith, D. M.; Chughtai, A. R. *Colloids Surf., A* **1995**, *105*, 47.

(14) (a) Tabor, K.; Gutzwiller, L.; Rossi, M. J. *Geophys. Res. Lett.* **1993**, *20*, 1431. (b) Tabor, K.; Gutzwiller, L.; Rossi, M. J. *J. Phys. Chem.* **1994**, *98*, 6172.

(15) Kalberer, M.; et al. *J. Phys. Chem.* **1996**, *100*, 15487.

(16) Hauglustaine, D. A.; Ridley, B. A.; Solomon, S.; Hess, P. G.; Madronich, S. *Geophys. Res. Lett.* **1996**, *23*, 2609.

(17) Lary, D. J.; Lee, A. M.; Toumi, R.; Newchurch, M. J.; Pirre, M.; Renard, J. B. *J. Geophys. Res.* **1997**, *102*, 3671.

(18) Bekki, S. *J. Geophys. Res.* **1997**, *102*, 10751.

(19) Thlibi, J.; Petit, J. C. In *Impact of Emissions from Aircraft and Spacecraft upon the Atmosphere*; Schumann, U., Wurzel, D., Eds.; Köln: Germany, 1994.

(20) Rogaski, C. A.; Golden, D. M.; Williams, L. R. *Geophys. Res. Lett.* **1997**, *24*, 381.

(21) (a) Chu, L. T.; Leu, M.-T.; Keyser, L. F. *J. Phys. Chem.* **1993**, *97*, 7779. (b) Chu, L. T.; Leu, M.-T.; Keyser, L. F. *J. Phys. Chem.* **1993**, *97*, 12798.

(22) Howard, C. J. *J. Phys. Chem.* **1979**, *83*, 3.

(23) *Handbook of Chemistry and Physics*, 65th ed.; Weast, R. C., Ed.; CRC Press: Boca Raton, FL, 1984.

(24) Technical Data: *Pigment Blacks*; Degussa: Ridgefield Park, NJ, 1996.

(25) (a) Leu, M.-T.; Timonen, R. S.; Keyser, L. F.; Yung, Y. L. *J. Phys. Chem.* **1995**, *99*, 13203. (b) Leu, M.-T.; Timonen, R. S.; Keyser, L. F. *J. Phys. Chem.* **1997**, *101*, 278.

(26) Cotton, F. A.; Wilkinson, G. *Advanced Inorganic Chemistry*, 5th ed.; Wiley-Interscience: New York, 1988.

(27) Atkins, P. W. *Physical Chemistry*, 3rd ed.; Freeman: New York, 1986.

(28) Mcbain, J. W.; Britton, G. T. *J. Am. Chem. Soc.* **1930**, *52*, 2198.

(29) (a) Keyser, L. F.; Moore, S. B.; Leu, M.-T. *J. Phys. Chem.* **1991**, *95*, 5496. (b) Keyser, L. F.; Leu, M.-T.; Moore, S. B. *J. Phys. Chem.* **1993**, *97*, 2800.

(30) Fenter, F. F.; Caloz, F.; Rossi, M. J. *J. Phys. Chem.* **1996**, *100*, 1008.

(31) Zhang, R.; Leu, M.-T.; Keyser, L. F. *J. Phys. Chem.* **1994**, *98*, 13563.

(32) Chatfield, R. B. *Geophys. Res. Lett.* **1994**, *21*, 2705.

(33) Jayne, J. T.; Worsnop, D. R.; Kolb, C. E.; Swartz, E.; Davidovits, P. *J. Phys. Chem.* **1996**, *100*, 8015.

(34) Horváth, M.; Lengyel, I.; Bazsa, G. *Int. J. Chem. Kinet.* **1988**, *20*, 687.